Available online at www.sciencedirect.com

ScienceDirect

Procedia CIRP 117 (2023) 426–431

www.elsevier.com/locate/procedia

19th CIRP Conference on Modeling of Machining Operations

Multiscale simulation approach to predict the penetration depth of oil between chip and tool during orthogonal cutting of AISI 4140

Florian Sauer[a*], Andrea Codrignani[b], Matthias Haber[c], Kerstin Falk[b], Leonhard Mayrhofer[b], Corina Schwitzke[c], Michael Moseler[b], Hans-Jörg Bauer[c], Volker Schulze[a]

[a]*wbk Institute of Production Science of Karlsruhe Institute of Technology (KIT), Karlsruhe, Germany*
[b]*IWM Fraunhofer Institute for Mechanics of Materials, Freiburg, Germany*
[c]*ITS Institute of Thermal Turbomachinery of Karlsruhe Institute of Technology (KIT), Karlsruhe, Germany*

* Corresponding author. Tel.: +49 721 608-44288. E-mail *address:* florian.sauer@kit.edu

Abstract

Cooling lubricants in machining perform important tasks, from cooling and lubrication of the friction partners in contact to the removal of the separated chips. An essential, determining and largely unresolved question in relation to cooling lubricants in machining is to what extent the coolant can get into the cutting zone. The aim of this paper is to address this question by using a multiscale approach to determine the penetration of the cooling lubricant gap. This is achieved by multiscale simulations by means of coupling the results of flow, structural and continuum mechanical simulations. Comparatively, the results of the simulated machining operation are compared with experimental orthogonal cutting tests of AISI 4140.

Keywords Finite element method (FEM), Lubrication, Cutting

1. Introduction

The cooling lubricant takes a major role in machining, by reducing the heat flow [1] into the tool and the friction in the contact area [2]. For cyclic engagement of the tool, as in the case of milling, this may lead to an increase in tool life [3] and ensures a reliable chip transport and good surface quality. However, the use of oil in the high productive gear manufacturing process gear skiving shortens the service life of the tools used in machining of AISI 4140 and AISI 4340 compared to dry machining [4]. These findings cannot yet be clearly described due to the complex kinematics, by means of highly variable cutting conditions during the tool engagement [5]. Therefore, the gear skiving process results in complex chip-tool interaction as well as in manifold multiscale interaction of fluid, structure and molecular dynamics. Studies of single-scale gear skiving without consideration of the cooling lubricant using FEM result in long calculation times [6]. Considering the complex interactions and the high computation times, it is therefore attempted to represent them by analogy tests in a simple 2D analysis model in order to provide the basis for a validated 3D simulation. It is assumed that a machining tribological system consists of 2 zones: the sticking zone and the sliding zone [7]. This is characterized by the sliding speed of friction partners and local normal stresses [8]. Furthermore, the contact length of the friction partners plays a major role. Studies showed that the real contact length is not influenced by the use of cooling lubricant in orthogonal cuts. This means that the size of the sticking zone is independent of the cooling and lubrication strategy [9]. In addition, Tabor et al. [10] proposed that the penetration of the cooling lubricant is low due to the relative speed of the chip and the locally high pressures in the contact. This raises the question of the extent to which the influence of the cooling lubricant in metalworking affects the existing frictional properties and its penetration into the cavity between the tool

10.1016/j.procir.2023.03.072

and the workpiece.

This paper aims to predict the distribution of the oil in the contact area based on orthogonal cutting experiments of AISI 4140 using oil as cooling lubricant considering the cutting conditions of a previously analyzed gear skiving process [4]. For this purpose, a multiscale simulation approach by means of CFD, FEM and Reynolds equations is used the first time to describe the dry contact length of the tool on the basis of the geometric and process boundary conditions.

2. Materials and Experimental Setup

The tests were carried out with samples from AISI 4140. The manufactured specimens with dimensions 100x50x4mm (LxWxD) were previously quenched and tempered at 600°C for one hour according to DIN 10083. The resulting hardness is 339±10 HV30 which, according to DIN EN ISO 18265, results in a tensile strength of 1070 ± 31MPa. The chemical composition of the material is given in Table 1.

Table 1. Chemical composition of AISI 4140 steel (wt %)

C	Mn	Si	P	S	Cr	Mo	Cu
0.41	0.81	0.33	0.01	0.023	1.04	0.189	0.13

Orthogonal cutting tests were performed on a 5-axis CNC milling machine of type MAG NBH 630 MT as shown in Figure 1. Hereby the tool holder is clamped into the tool spindle. Different rake angles can be set by turning the tool spindle.

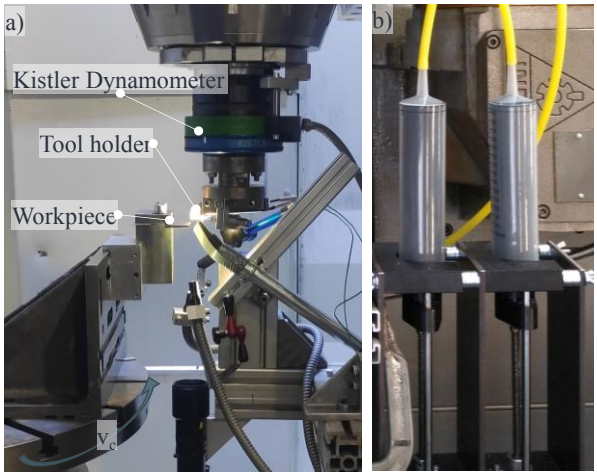

Figure 1. Orthogonal test set up; a) detail of tool and workpiece; b) stepper motors .

The workpiece is clamped on the rotary table. By rotating the table, the cutting speed can be adjusted. The cutting and passive forces during machining were measured and recorded with a Kistler Type 9124B1011 mounted in the machine spindle at a sampling frequency of 10 kHz. Coated tungsten carbide tool inserts of the type CCMW120404 with a rake angle $\gamma = 0°$, a clearance angle, $\alpha = 7°$, and a cutting edge radius, $r_\beta = 30$ µm, without chip breaker were used for the tests. These cutting tools are coated with an AlCrN-based layer from the company Oerlikon Balzers. To avoid the influence of wear, the cutting inserts were only used once per trial number. The additive-free paraffinic-base oil "TUDALEN 3036" was used as cutting fluid, which was applied to the cutting zone by means of a syringe design controlled by stepper motors (see Figure 1b). The set flow rate lies at 1 l/min with a nozzle diameter of 2 mm. The cooling nozzle points directly at the cavity formed between the chip and the tool. The main pourpose of this study is to represent the challenging cutting conditions of gear skiving by means of an orthogonal cutting set-up. Therefore, the cutting speeds, rake angles, and chip thicknesses were exported as parameter fields using the freely available software OpenSkiving [11] to analyse the manufacturing of a ring gear from e-mobility application [4]. Given the parameter field the maximum and minimum values were extracted and transferred into a fully factorial test design (Table 2).

Table 2. Full factorial designs of experiments

Trial Number -	Cutting speed in m/min	Uncut chip thickness in µm	Rake angle in °
1	115	50	-25
2	140	50	-25
3	115	150	-25
4	140	150	-25
5	115	50	-5
6	140	50	-5
7	115	150	-5
8	140	150	-5
9	127.5	100	-15

3. Numerical Modelling

To determine the penetration of the fluid in the cavity between the workpiece and the tool, the input data from 2D FE simulations and CFD simulations are required. The individual simulation models of the orthogonal cut extract the following data by means of a loose coupling method (Figure 2). After the chip formation simulation, the geometrical boundary conditions are transferred to the CFD simulation in order to determine the fluid pressure distribution in the cutting area which in turn is provided as input for the Reynolds equation solver (RES). Further, the FE simulation passes on the data to the RES in the way of sliding velocity and normal pressure distribution of the friction partners. Finally, the fluid distribution in the contact area between tool and workpiece is predicted by means of Reynolds equation.

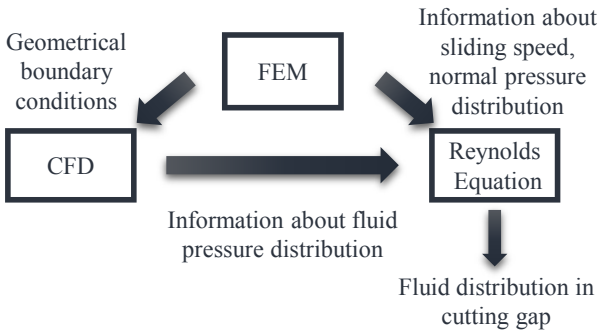

Figure 2. Data transfer between simulation models

3.1. FE-Simulation

2D-FEM simulation was carried out for the nine different experimental point by using the FE software Simufact Forming 21, which is based on MSC Marc 2019 [12]. The model was set up with a mesh type of quadrilateral elements with a plain strain assumption and continuous re-meshing depending on refinement boxes, element distortion and strain change resulting in a minimum element edge length of 8 µm. Due to the continuous re-meshing the simulation was performed as an implicit time integration. The simulation included a rigid tool fixed in the space, an elasto-plastic workpiece, and two heat sink fixed bodies for the workpiece and the tool as shown in Figure 3.

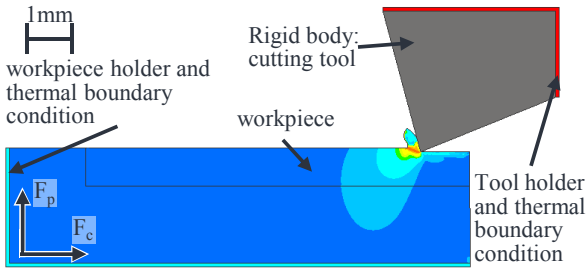

Figure 3. FE-Model setup.

The friction behaviour between the workpiece and the cutting edge was described as a combined Coulomb-shear friction law (Eq. 1). Where τ_f refers to the contact shear stress, σ_n refers to the contact normal stress, μ refers to the Coulomb friction coefficient, and τ refers to the shear friction coefficient.

$$\tau_f = \begin{cases} \mu \cdot \sigma_n \text{ when } \mu \cdot \sigma_n < \sigma_f \\ m \cdot \sigma_n \text{ when } \mu \cdot \sigma_n > \sigma_f \end{cases} \quad (1)$$

The Coulomb value μ and the shear factor m were fixed at 0.35 and 1 as obtained in previous works [13]. The Johnson-Cook plasticity model (Eq. 2) was used to model the workpiece material [14].

$$\sigma_f = [A + B\bar{\varepsilon}^n]\left[1 + C \ln\left(\frac{\dot{\varepsilon}}{\dot{\varepsilon}_0}\right)\right]\left[1 - \left(\frac{\theta - \theta_{room}}{\theta_m - \theta_{room}}\right)^m\right] \quad (2)$$

The model parameters are given in Table 3, where A is the yield strength, B is the hardening modulus, C is the strain rate sensitivity coefficient, n is the hardening coefficient and m the thermal softening coefficient [13].

Table 3. Johnson-Cook Parameter

A in MPa	B in MPa	C	n	m
595	580	0.023	1.03	0.133

The cutting edge rounding was set to 30 µm, measured optically with a Keyence VHX-970f by observing the real geometry. Parameters kept constant for the simulation are given in Table 4.

Table 4. Constant parameters of the FE-Simulation

θ_m K	θ_{room} K	λ_c W/mK	$\dot{\varepsilon}_0$ -	α_{air} W/m²K
1820	293	120	1	50

Here α_{air} refers to the heat transfer coefficient between the tool/workpiece and the environment, θ_{room} is the ambient temperature and the reference temperature for the Johnson-Cook placticity model, θ_m is the melting temperature, and $\dot{\varepsilon}_0$ is the reference strain rate, see Eq. 2. To obtain sliding velocities and the distribution of the contact pressure on the rake face of the tool, the values were exported by means of a Fortran subroutine for the use in the Reynolds equation. The needed updated geometrical workpiece and cutting tool were exported as STL-files with a minimum element-edge length of 0.15 µm for the CFD-simulations.

3.2. CFD-Simulation

To evaluate the distribution of the fluid, the velocity field and the pressure of the cutting fluid close to the chip-tool-contact, Smoothed Particle Hydrodynamics (SPH) simulations are conducted. The method uses a purely Lagrangian formulation of the Navier-Stokes equations. Therefore, the computational domain is discretized by movable particles, which store the quantities of the fluid flow at discrete spatial points. To reduce computational effort, the kernel function is truncated at a maximum radius of influence. Only particles within this sphere of influence participate in the simulation. In the conducted simulation a Quintic spline kernel is applied with a smoothing length of $h = \Delta x$ and a maximum influence radius $r_{max} = 3h$. Δx represents the mean particle spacing. Furthermore, a Single-Phase formulation is used, where the cutting fluid is discretized by particles while the surrounding air is not represented. Neglecting the air-phase reduces tremendously the computational cost [15]. Considering the setup presented here, the Single-Phase formulation is applicable due to the comparatively low air velocities and the small distance of the nozzle outlet to the impact compared to the jet diameter. The investigated 2D geometry is imported from the cutting simulations. The workflow of the simulation is carried out exemplarily for one operating point (Trial number 9 cf. Table 2). The walls of the domain (workpiece, chip, tool and nozzle) are discretized by three layers of particles to provide a sufficient kernel support. The motion and growth of the chip is slow compared to typical velocities of the cutting fluid. Hence, growth of the chip is neglected and the geometry is extracted from certain time steps of the cutting simulation. For the simulations carried out, the most significate variables summarized in Table 5 are analysed. First, the resolution is varied by means of two different mean particle spacing. Next, the influence of the chip geometry is investigated by picking different time steps of the cutting simulation. Finally, the influence of the nozzle diameter and volume flow rate of cutting fluid is investigated. The distance of the nozzle outlet to the tool tip is kept constant to 9 mm for all simulations.

Table 5 Conducted simulations

# -	cutting path mm	Particle spacing µm	Volume flow rate l/min	Nozzle diameter mm
A	2.4	10	1.0	2
B	2.4	25	1.0	2
C	0	10	1.0	2
D	6.9	10	1.0	2
E	2.4	10	1.5	1
F	2.4	10	3.0	2

3.3. Pressure Probing

Figure 4a. shows the results of the cutting fluid distribution and the total pressure field for simulation F in the vicinity of the chip. The results are extracted, when the cutting fluid reaches a steady state distribution. Besides some small fluctuations in the pressure field the cavity is completely filled with fluid. An unphysically high pressure rise in the very thin gap formed by the chip-tool contact can be observed, due to approximation errors of the SPH schemes with low particle number and errors in the surface tension model for sharp edges. Therefore, the pressure probing location is shifted to the area indicated by the green circle with a spatial averaging of the values of pressure. Figure 4b reveals, that this shift is not crucial regarding physical distribution of pressure. The velocity magnitude is almost zero within the probing region. A further deceleration closer to the gap will not increase the dynamic pressure and consequently not increase the applied pressure.

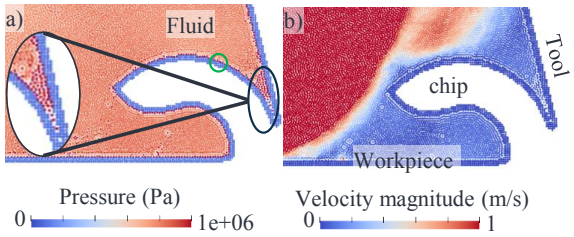

Figure 4. a) Typical pressure distribution with highlighted area of probing b) Velocity field in vicinity of the chip

3.4. Reynolds calculation

The penetration depth of the coolant into the interface region between the tool and the developing chip of the workpiece was calculated using the Reynolds equation with a mass conserving cavitation model as shown in Eq. 3 [16].

$$\nabla \cdot \left[-\frac{\rho h_f^3}{12\mu_f} \nabla \bar{p} + \frac{1}{2} \rho h_{ref} U_{chip} (1-\theta) \right] = \nabla [q_r - q_l] = 0 \tag{3}$$

where: $\theta = 1 - \frac{\rho}{\rho_{ref}}$, $\bar{p} = p - p_{ref}$ $\bar{p} \cdot \theta = 0$

Where μ_f and ρ indicate the viscosity and density of the oil, p the pressure distribution at the chip cavity, h_f the film thickness, U_{chip} the relative sliding velocity, h_{ref}, p_{ref} and ρ_{ref} are indicating the reference film thickness, pressure and density. The cavity fraction is given by θ and q_r and q_l are indicating the mass flow of the set boundaries. The geometry of the simulated system is shown in Figure 5. The cooling lubricant enters from the right side with pressure $p = 0.6$ MPa (boundary condition set according to the CFD simulation results). The fluid viscosity value of $\eta = 0.045$ Pa·s, was the determined according to DIN EN ISO 3104. The calculation was performed with two main parameters, namely the speed, U_{chip} of the chip with respect to the tool, and the minimum height, $h_{\min}$ of the gap between tool and chip. The latter was defined to account for the uncertainty in the gap size and the roughness of the real measured experimental system. In order to describe quantitatively how far the coolant (MWF) can penetrate into the contact, the so-called dry length L_{dry} was defined, which represents the length of the dry region of the chip-tool interface as sketched in Figure 5.

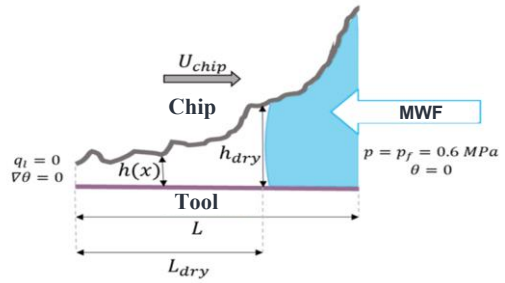

Figure 5. Geometry of the Reynolds calculation

4. Results

4.1. FE-Simulation Results

The local values of the relative sliding velocity and normal pressures in the chip-tool contact for the full factorial test plan presented in Table 2 are shown in Figure 6. According to the results presented by Bergmann [8], the extracted simulation results show a typical progression of the indicated values.

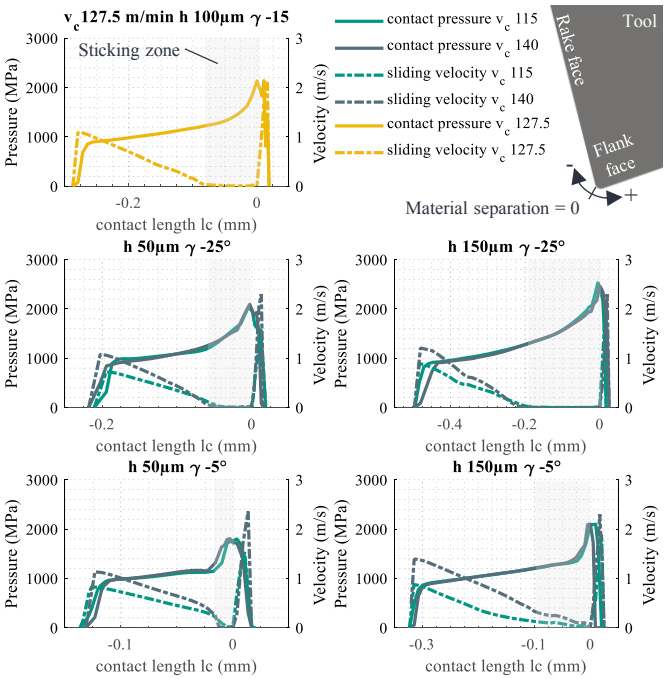

Figure 6. Relative sliding velocities and normal contact pressure in the contact area of the investigated full factorial test setup

A linear decrease of the sliding velocity up to a relative velocity of 0 m/s appears at all investigated points. This indicates the beginning of the sticking zone of the tribological contact, which continues until material separation at the cutting edge radius and is characterized by a low material flow rate (shadowed area). For the normal stresses in the contact, a steep gradient can be seen at the beginning of the contact area. Subsequently, a linear increase of the normal stress up to the beginning of the sticking zone is observed for the investigated parameter sets. As soon as the sticking zone is reached in the tribological contact due to the relative speed of 0 m/s, the normal stress increases with a larger gradient. Depending on the examined uncut chip thickness, this increase occurs in different distinct. In particular, the smaller the rake angle applied, the more evident the increase in normal stress at the beginning of the sticking zone. The highest normal stresses occurs in the area of the cutting edge rounding. Up to the material separation point, the relative sliding velocities are equal to 0 m/s. After the material separation point (indicated in Figure 6 as 0), the relative sliding velocities increase again stepwise to almost the applied cutting velocities, resulting in a high velocity gradient. At the same time, the normal stress presents decreases after the material separation point. However, for the investigated parameter set, different characteristics can be observed: Thus, in the case of a negative rake angle, the tool-chip contact length increases while the uncut chip thickness remains the same. This also results in a larger sticking zone in the tribological contact. For instance, a reduction of the rake angle from -25° to -5° reduces the contact length by approx. 50%, irrespective of the selected chip thickness. In addition, the local stress on the cutting edge is reduced by the reduction of the normal stress. The lower shear rates and the reduced shear angle are the main factors for this. Furthermore, the influence of the cutting speed has a small effect on the normal stress distribution but a high impact on the relative sliding velocities. In summary, rake angle and chip thickness have the greatest influence on the present

parameters of normal stress distribution, which directly influences the formation of the sticking zone and thus the present tribological conditions.

4.2. CFD-Simulation Results

At first, the necessary resolution of particles is analysed by comparison of simulations (A) and (B). For this purpose, the geometry of the cutting simulations after 2.4mm cutting path is used. A nozzle of 2 mm in diameter is placed in the domain, pointing directly at the cavity between tool and chip. The flow rate is set to 1 l/min at the nozzle velocity inlet. Figure 7 a) and b) shows a comparison of the velocity fields and fluid distributions for the $\Delta x = 25$ µm and $\Delta x = 10$ µm. The evaluation is done after the cutting fluid distribution remains in a steady state. The distributions and the velocity field look very similar. From this perspective the medium resolution (B) is the preferable. Nevertheless, the finest resolution is chosen, because of the better discretization of the gap area as reference configuration. Furthermore, three states of the chip formation are investigated. Simulation (D) uses the initial state of the cutting simulation of the undeformed workpiece, whereas simulation (E) takes one of the last time steps. In Figure 7 c) and d) the velocity fields and cutting fluid distributions of simulation (D) and (E) can be compared. The reference simulation (A) in a) should also be considered. The results of all three simulations look very similar. In the cavity, a region of low velocity forms. Consequently, a minor influence of the chip geometry on the flow characteristics is observed. It can be explained by the small length scale of the chip compared to the nozzle diameter and especially compared to the flood area.

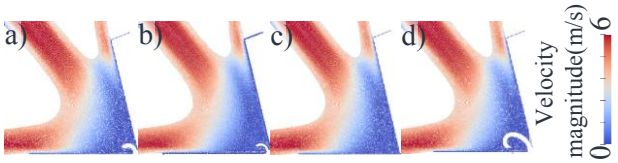

Figure 7. Cutting fluid distribution and velocity fields for a) $\Delta x = 10$ µm; b) $\Delta x = 25$ µm; c) FE time step 0; d) FE time step 31.

The main objective of the SPH simulations is to provide a static pressure in the vicinity of the gap by probing and spatially averaging particle values in the continuum scale. Since the geometry of the chip has minor influence on the flow characteristics, only the influence of the volume flow rate and the nozzle diameter are investigated. Exemplarily the total pressure distribution of simulation (F) is shown in Figure 8 a). It reveals the same flow characteristics as pointed out before. A region of high pressure (and corresponding low velocity magnitude) is formed in the cavity in vicinity to the chip.

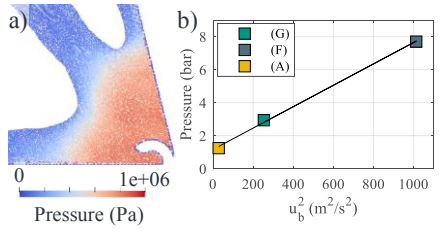

Figure 8. a) Cutting fluid distribution and pressure field for simulation (F); b) Pressure over squared bulk velocity

To validate the simualiton results, the determined pressures are plotted against the square of the dynamic velocity (Figure 8b). The relation can be determined by the Bernoulli equation for the calculation of the dynamic pressure. To do this the pressure close to the chip is related to the sum of the dynamic pressure of the nozzle flow and the static ambient pressure. The square function can thus be used to calculate the pressure boundary conditions for the Reynolds-Equation solver.

4.3. Reynolds Equation Results

The Reynolds simulations of the innermost part of the chip-tool contact result in the dry length, i.e. the length of the contact region which is not penetrated by the cooling lubricant. The results for the dry length (normalized by the total length of the model system) are shown in Figure 9. The dry length is almost independent of the minimum gap height, but it increases with the chip velocity. For velocity values, which are typical for the studied orthogonal cutting process (~1m/s) the fluid cannot reach the innermost about 28% of the contact. This result can be used in a friction model of the full contact to separate the dry and the lubricated region.

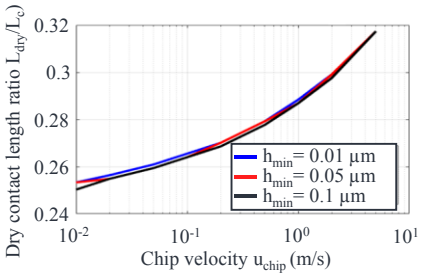

Figure 9. Dry length of the chip/tool contact from Reynolds calculation

The calculated dry contact ratio in conjunction with the extracted contact length results from the FE simulation can finally be used to determine the dry length in the investigated point of testing. The comparison between the dry length predicted by the Reynolds equation and the FE-simulated sticking zone in the contact area is shown in Figure 10. The averaged values obtained from the ratio of the calculated dry length using the Reynolds equation and the sticking zone determined by FE simulations of the investigated points show good agreement. In particular, for large chip thicknesses ($h = 150$ µm) with small rake angles ($\gamma = -5°$), for small chip thicknesses ($h = 50$ µm) and highly negative rake angles ($\gamma = -25°$), as well as for the central point of the test plan ($h = 100$ µm, $\gamma = -15°$) the dry length is equal to the determined sticking zone in the tribological contact. For small chip thicknesses ($h = 50$ µm) with small rake angles ($\gamma = -5°$) as well as for large chip thicknesses ($h = 150$ µm) and highly negative rake angles ($\gamma = -25°$), a larger deviation is observed, whilst these investigated points have an opposite trend.

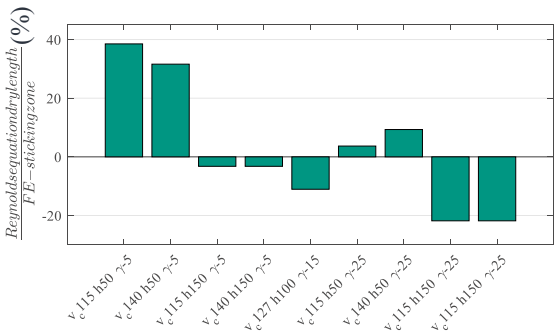

Figure 10. Percentage deviation of sticking zone to dry length

4.4. Experimental results

The measured cutting and passive forces for dry orthogonal cut and oil lubricated are compared to the achieved simulation results with dry friction parameters in Figure 11 and in Table 6 the percentage deviation related to dry results. Cutting forces increase with increase of the uncut chip thickness and increased negative rake angles. The measured results indicate that the application of oil in the orthogonal cut has no influence on the measured forces of the cutting and passive forces. Considering that, the cutting forces are dependent on the contact length and normal stresses, this confirms the calculations using the Reynolds equation of the dry length. In particular, since the normal stresses are highest in the range of the dry length and thus have a great influence on the calculated cutting forces. In addition, the simulation results show good agreement with the experimental data for the cutting and passive force. In detail, the cutting forces are overestimated for highly negative rake angles and underestimated for less steep rake angles. This behaviour shows an opposite trend in the passive force. Overall, a good agreement of the considered parameter range appears, which thus serves as a validation of the extracted values.

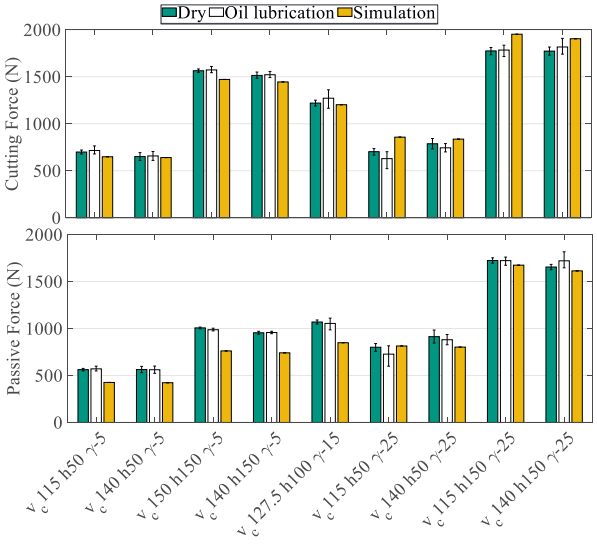

Figure 11. Cutting- and passive force comparison between dry, oil lubricated and simulations results

Table 6 Comparison of test results with dry, oil lubricated and simulation results as percentage as percentage deviation

	cutting velocity (m/min)	115	140	115	140	127.5	115	140	115	140	average deviation
	Uncut chipthickness (µm)	50	50	150	150	100	50	50	150	150	
	Rake Angle (°)	-5	-5	-5	-5	-15	-25	-25	-25	-25	
cutting force	Dry	-	-	-	-	-	-	-	-	-	-
	Oil lubrication	2%	1%	1%	0%	4%	-11%	-5%	1%	2%	100%
	Simulation	-7%	-2%	-6%	-5%	-1%	22%	6%	10%	7%	103%
passive force	Dry	-	-	-	-	-	-	-	-	-	-
	Oil lubrication	2%	0%	-2%	0%	-1%	-9%	-4%	0%	4%	99%
	Simulation	-24%	-25%	-24%	-22%	-21%	2%	-12%	-3%	-2%	85%

5. Conclusion

The formation of the dry length during the machining of AISI 4140 with the use of oil has been investigated by means of simulation and validated with experimental results in orthogonal cutting. The key findings of this work are:

- The dry contact length is almost independent of the minimum gap height, but increases with increasing relative sliding speed.
- The pressure distribution of the fluid at the tool-workpiece contact is uniform and linear to the bulk velocity.
- The determined dry contact length, calculated with Reynolds equation corresponds to the determined FE-Simulation of the sticking zone in the tool contact.
- For typical cutting velocities in wet gear skiving, about 26-32% of the tool-chip contact remains dry.

Acknowledgement

The authors gratefully acknowledge the funding of this work within the Priority Program 2231 "Efficient Cooling, Lubrication and Transport-Coupled Mechanical and Fluid Dynamic Simulation Methods for Efficient Production Processes (FLUSIMPRO)" by the German Research Foundation (DFG)-Project no. SCHU 1010, BA 2848 and MO 879.

References

[1] F. Klocke, A. Krämer, H. Sangermann, and D. Lung, "Thermo-mechanical tool load during high performance cutting of hard-to-cut materials," *Procedia CIRP*, vol. 1, no. 1, pp. 295–300, 2012, doi: 10.1016/j.procir.2012.04.053.

[2] B. Peng, T. Bergs, D. Schraknepper, T. Smigielski, and F. Klocke, "Development and validation of a new friction model for cutting processes," *Int. J. Adv. Manuf. Technol.*, vol. 107, no. 11–12, pp. 4357–4369, 2020, doi: 10.1007/s00170-019-04709-8.

[3] A. Oladeji, M. Bose, A. Ushe, A. Rahmat, and M. Biola, "Influence of Cutting Fluid on Machining Processes : A Review," vol. 34, no. 3, pp. 365–373, 2022.

[4] F. Sauer, T. Arndt, and S. Volker, "Tool wear development in gear skiving process of different quenched and tempered internal gears," *VDI-4th Int. Conf. Gear Prod. 2022*, vol. 2389, pp. 1331–1343, 2022.

[5] A. Hilligardt and V. Schulze, "A holistic approach for gear skiving design enabling tool load homogenization," *CIRP Ann.*, vol. 71, no. 1, pp. 85–88, 2022, doi: https://doi.org/10.1016/j.cirp.2022.03.029.

[6] V. Schulze, C. Kühlewein, and H. Autenrieth, "3D-FEM modeling of gear skiving to investigate kinematics and chip formation mechanisms," *Adv. Mater. Res.*, vol. 223, pp. 46–55, 2011, doi: 10.4028/www.scientific.net/AMR.223.46.

[7] A. Malakizadi, K. Hosseinkhani, E. Mariano, E. Ng, A. Del Prete, and L. Nyborg, "Influence of friction models on FE simulation results of orthogonal cutting process," *Int. J. Adv. Manuf. Technol.*, vol. 88, no. 9–12, pp. 3217–3232, 2016, doi: 10.1007/s00170-016-9023-4.

[8] B. Bergmann, B. Denkena, S. Beblein, and T. Picker, "FE-simulation roundings based design of wear-optimized cutting edge roundings," *J. Manuf. Mater. Process.*, vol. 5, no. 4, 2021, doi: 10.3390/jmmp5040126.

[9] L. Ellersiek, C. Menze, F. Sauer, B. Denkena, H. C. Möhring, and V. Schulze, "Evaluation of methods for measuring tool-chip contact length in wet machining using different approaches (microtextured tool, in-situ visualization and restricted contact tool)," *Prod. Eng.*, no. 0123456789, 2022, doi: 10.1007/s11740-022-01127-w.

[10] J. A. Williams and D. Tabor, "The role of lubricants in machining," *Wear*, vol. 43, no. 3, pp. 275–292, 1977, doi: https://doi.org/10.1016/0043-1648(77)90125-9.

[11] "OpenSkiving." [Software] KIT Campus Transfer GmbH, Karlsruhe, 2022.

[12] "Simufact Forming (2021)." simufact engineering gmbh, Hamburg, 2021.

[13] B. Stampfer, G. González, E. Segebade, M. Gerstenmeyer, and V. Schulze, "Material parameter optimization for orthogonal cutting simulations of AISI4140 at various tempering conditions," *Procedia CIRP*, vol. 102, pp. 198–203, 2021, doi: 10.1016/j.procir.2021.09.034.

[14] G. R. Johnson and W. H. Cook, "A Computational Constitutive Model and Data for Metals Subjected to Large Strain, High Strain Rates and High Pressures," *Seventh Int. Symp. Ballist.*, pp. 541–547, 1983.

[15] M. C. Keller *et al.*, "Smoothed Particle Hydrodynamics Simulation of Oil-Jet Gear Interaction1," *J. Tribol.*, vol. 141, no. 7, May 2019, doi: 10.1115/1.4043640.

[16] T. Woloszynski, P. Podsiadlo, and G. W. Stachowiak, "Efficient Solution to the Cavitation Problem in Hydrodynamic Lubrication," *Tribol. Lett.*, vol. 58, no. 1, 2015, doi: 10.1007/s11249-015-0487-4.